Quiles-Carrillo, L.; Montanes, N.; Boronat, T.; Balart, R.; Torres-Giner, S. (2017). Evaluation of the engineering performance of different bio-based aliphatic homopolyamide tubes prepared by profile extrusion. Polymer Testing. 61:421-429. https://doi.org/10.1016/j.polymertesting.2017.06.004

Evaluation of the engineering performance of different bio-based aliphatic homopolyamide tubes prepared by profile extrusion

L. Quiles-Carrillo [a], N. Montanes [a], T. Boronat [a], R. Balart [a] and S. Torres-Giner [b,c*]

[a] ***Technological Institute of Materials (ITM)***, *Universitat Politècnica de València (UPV), Plaza Ferrándiz y Carbonell 1, Alcoy 03801 Spain*

[b] ***Novel Materials and Nanotechnology Group***, *Institute of Agrochemistry and Food Technology (IATA), Spanish Council for Scientific Research (CSIC), Calle Agustín Escardino Benlloch 7, Paterna 46980 Spain*

[c] ***School of Technology and Experimental Sciences (ESTCE)***, *Universitat Jaume I (UJI), Avenida de Vicent Sos Baynat s/n, Castellón 12071 Spain*

****Corresponding authors**: S. Torres-Giner (storresginer@iata.csic.es and storresginer@hotmail.com*)

ABSTRACT. In the present study, three different commercial bio-based polyamides (bio-PAs), namely polyamide 610 (PA610), polyamide 1010 (PA1010), and polyamide 1012 (PA1012), were processed by profile extrusion with an annular die. These aliphatic homopolyamides, also known as "green nylons", are industrially produced by polycondensation reaction of diamines and dicarboxylic acids that are partially or fully obtained from naturally occurring castor oil. The profile-extruded bio-PA tubes were characterized and compared in terms of their thermal, thermomechanical, and mechanical properties and water uptake. Resultant comparative evaluation indicated that both the methylene-to-amide (CH_2/CONH) ratio and the crystallinity degree of the bio-PAs played the main role in determining the tube properties. Due to significant differences in their CH_2/CONH ratio, the PA610 tubes showed the highest thermal performance while the tubes made of PA1012 tubes presented the highest flexibility and lowest water uptake. Interestingly, the fully bio-based PA1010 tubes offered the most balanced and enhanced engineering performance, which was ascribed to the high crystallinity achieved during profile extrusion. The here-developed bio-PA tubes can fulfil demanding technical requirements and these also certainly represent a sustainable answer to the rising demand for new high-performance biopolymers for engineering applications

KEYWORDS Green nylons; Methylene-to-amide ratio; Plastics engineering; Structure-property relationships; Tubing extrusion

1. Introduction

Polyamides are polymers, generally linear and semi-crystalline, with recurring amide groups as an integral part of the main polymer chain. These are commonly known in the plastics industry as “nylons”, which are referred to any polyamide having less than 85% of the amide groups directly connected to two aromatic groups [1]. Discovered by Wallace Carothers and early commercialized in the 1940s by DuPont, polyamides can be either obtained by ring-opening polymerization (ROP) of lactams, *i.e.* their bi-functional monomer, or polycondensation, *i.e.* condensation polymerization of diamines and diacids at elevated temperature [2]. The latter reaction is based on a “nylon salt” solution, where the corresponding salt is previously formed at room temperature using a molar ratio dicarboxylic acid/diamine 1:1. The amide group, along with its essential structural role, contributes to the extraordinary mechanical strength and thermal resistance of polyamides due to its polar nature and high chemical stability. As a result, these thermoplastic materials are traditionally considered as “engineering plastics”, being currently manufactured for a wide variety of technically demanding applications such as fibers for clothing for carpets, injection-molded car parts, oil delivery lines and gas pressure pipes, barrier films for food packaging, and soles for high-quality sports shoes [3]. Nowadays, the global plastics market annually requires over 6 million tons of polyamides with a growing rate close to 5% [4]. Traditional polyamide 6 (PA6) and polyamide 66 (PA66), and recently polyamide 12 (PA12), constitute more than 90% of their overall usage in the plastics industry [5].

Even though high-performance plastics are classical petrochemistry products, polymer chains can also be partially or completely synthesized from bio-based components [6]. In particular, the development of a sustainable route to the production of bio-based polyamides (bio-PAs) has recently received a high interest due to the growing awareness of the damage sustained by environment [7]. In particular, the synthesis of both traditional and new polyamides from renewable resources could exceptionally reduce high amounts of fossil energy, which is particularly favorable in the light of the growing shortage and rising price of fossil resources[8]. Unfortunately, the use of fully bio-PAs, excluding polypeptides and proteins, is still restricted

due to the limited availability of renewable diamines [9]. Thus, increasing the applications of bio-PAs is certainly of major interest.

Without doubt, castor oil is nowadays playing the biggest role as the raw material to yield the building blocks for the production of bio-PAs [10]. This is a natural, viscous, pale yellow, non-volatile, and non-drying oil with an unusual homogeneous composition. Structurally, castor oil contains 85–95% ricinoleic acid, a 18-carbon (C18) fatty acid, which is available in its triglyceride ester [11]. The oil is obtained from the seed of the *Ricinus communis* plant, which belongs to the family Eurphorbiacae and predominantly grows in the wild of tropical and subtropical countries (*e.g.* Africa, India, Brazil, and China) [12]. Castor oil is not only a naturally occurring resource, but it is also inexpensive and environmentally friendly. Due to its extreme drought resistance, the plant is primarily cultivated in sites that are unsuitable for food production so that it does not compete directly with food purposes [13]. It is estimated that over 600,000 metric tons of castor oil are annually produced, of which at least one third are currently used for the synthesis of bio-PAs [14].

Ricinoleic acid is the starting compound for the different bio-routes, which is obtained by subjecting castor oil either to a transesterfication step or a saponification step [15]. Sebacic acid, *i.e.* 1,10-decanedioic acid, is manufactured by heating ricinoleic acid to high temperatures, typically about 250°C, with alkali [16]. Although its manufacturing yields are lower than those of current petrochemical monomers used in the synthesis of traditional polyamides, this route has been found to be cost competitive [17]. The C10 dicarboxylic acid can readily react with petroleum-based 1,6-hexamethylene diamine (HMDA), obtained from butadiene, *via* polycondensation to produce aliphatic polyamide 610 (PA610). As a result, PA610 is typically 60–63 wt.-% based on natural resources [18]. Sebacic acid can also polymerize with 1,10-decamethylene diamine (DMDA) to produce aliphatic polyamide 1010 (PA1010). Interestingly, DMDA, the C10 diamine, can be obtained by exposing sebacic acid to ammonia followed by dehydration and hydrogenation [19]. Since both monomers are obtained from castor oil, resultant PA1010 is fully bio-based. Finally, aliphatic polyamide 1012 (PA1012) is a polycondensation product of DMDA and 1,12-dodecanedioic acid. The C12 dicarboxylic acid is

typically fossil-based, being the bio-based content of PA1012 approximately 45 wt.-%. However, more recently, this has been also obtained from palm kernel oil *via* a biotechnological process [20]. As a result, PA1012 can also consists up to 100 wt.-% of renewable raw materials. **Figure 1** shows the chemical structure of PA610, PA1010, and PA1012, indicating the weight percentage of renewably sourced ingredients. As it can be observed, these bio-PAs consist of amide groups separated by alkane segments of different length, which results in different amide concentration per polymer chain. Therefore, the methylene-to-amide (CH_2/CONH) ratio results in 7, 9 and 10 for PA610, PA1010 and PA1012, respectively. Polyamides with longer aliphatic segments, *i.e.* with higher CH_2/CONH ratios, have reasonably lower amide densities per unit length of chain. Interestingly, the CH_2/CONH ratio, in combination with the chain symmetry, is known to determine the final properties of polyamides [21]. Even-even polyamides form chain-folded sheets in which the amide groups participate in linear hydrogen bonding to one another. Lower CH_2/CONH ratios result in a density increase of hydrogen bonds, which restricts the segmental inter-chain mobility of the long-chain aliphatic methylene groups in the polymer backbone and then increases thermal resistance [21], mechanical strength and abrasive wear performance [22] and, hence, tribological behavior [23]. In addition, hydrogen bonding pulls many of the polyamide chains into more ordered crystalline regions, which further increases the polyamide melting point. In particular, it is considered that resultant hydrogen bonds are able to retain the polyamide chains in an ordered solid phase after the alkane segments have effectively melted [21]. Hydrogen bonding also takes place between polyamide and water or polar absorbed substances, which acts as a plasticizer, lowering the glass transition temperature (T_g) and impairing the mechanical performance significantly [24].

Profile extrusion is the high-volume process of making continuous shapes of plastic, ranging from solid to hollow forms, but not including sheet and film. When the polymer melt is extruded through an annular die, round cross-sections such as tubes and pipes are obtained. This is specifically called pipe extrusion or tubing extrusion [25]. During this process, polymer resins, habitually in the form of pellets, flow from the main hopper to the gap between the rotating screw and heated barrel of the extruder. Once the polymer is melted, mixed and

pressurized in the extruder, it is then pumped through the annular die. The extruded product, while being pulled, passes through a vacuum sizer in which it attains its final dimensions. This is followed by cooling *via* chilled water immersion or spraying and cutting to fixed lengths. Pipes, with a diameter of 2 m or greater, and tubes, from 10 mm down to below 1 mm, can be processed by profile extrusion [26]. The annular dies used in this process are normally of spider or spiral mandrel design [27].

The present study reports, for the first time, the preparation by profile extrusion and characterization of tubes made of three bio-PAs, namely PA610, PA1010, and PA1012. Since the amide group concentration controls the physical properties of aliphatic polyamides, the thermal, thermomechanical, and mechanical performance and water uptake of these bio-PA tubes were evaluated and compared. The obtained results were ascribed to the chemical structure of the bio-PAs, based on different CH_2/CONH ratios, and the processing conditions in which the tubes were obtained.

2. Experimental

2.1. Materials

PA610 was supplied by DuPont (Solingen, Germany) as medium-viscosity grade Zytel® RS LC4601. This homopolyamide is developed for extrusion applications, has a density of 1.04 g/cm^3, and contains approximately 60 wt.-% of renewably sourced ingredients. Commercial PA1010 was Grilamid® XE 4181 provided by EMS-Chemie A.G. (Domat/Ems, Switzerland). This is a fully bio-based high-viscosity extrusion-grade homopolyamide with a density of 1.05 g/cm^3. Finally, PA1012 was Vestamid® Terra DD 2230 (CW1120), distributed by Evonik Industries (Essen, Germany). This is a high-viscosity homopolyamide with a density of 1.03 g/cm^3 and 45 wt.-% based on bio-renewables. The renewable weight contents were provided by the manufacturers according to ASTM D6866 standard.

2.2. Profile extrusion

Extrusion of tubes was performed using a Collin E30M single-screw extruder equipped with a 15-mm annular die based on a spider ring design. The barrel extruder presented a

length/diameter (L/D) of 30 and screw speed was 40 rpm. Temperature profile was set accordingly to provide a melt temperature during extrusion of 250°C, for PA610, and 225°C, for PA1010 and PA1012. In all cases die temperature was set at 275°C. The process is illustrated in **Figure 2** showing its different sections. Briefly, the extruded tube exiting the die travelled a short distance in air, allowing a thin skin to form. Then it passed through a vacuum sizing chamber, which was equipped with sizing rings and operated at 230 mbar. The tubes, while being pulled, entered a cooling bath with chilled water at 15°C to dissipate the heat. The pull-out system was a caterpillar-type puller (capstan). Finally, annealing was performed in a reheat station working with an open flame. Line speed was 5 m/min. Tube specimens of different lengths with an outer diameter (OD) of 10 mm and wall thickness of 1 mm were ejected from the cutting station.

2.3. Infrared spectroscopy

Chemical analysis was performed *via* attenuated total reflection–Fourier transform infrared (ATR-FTIR) spectroscopy. Spectra were recorded using a Bruker S.A. Vector 22 (Madrid, Spain) coupled to a PIKE MIRacle™ single reflection diamond ATR accessory (Madison, USA). Data were collected as the average of ten scans from 4000 to 400 cm^{-1} at a spectral resolution of 4 cm^{-1}.

2.4. Thermal characterization

Thermal transitions were obtained by differential scanning calorimetry (DSC) using a Mettler-Toledo, Inc. (Schwerzenbach, Switzerland) 821 model. For this, *ca.* 5 mg of tube samples were placed in 40-µl hermetic aluminum sealed pans, previously calibrated with an indium standard. The analysis was performed in a dry reducing atmosphere in which nitrogen flowed at a constant rate of 66 mL/min. Samples were subjected to a two-step regime at a heating rate of 10 °C/min to evaluate the thermal transitions. An initial heating scan from 30 to 250°C was followed by a cooling scan to 30°C. The cold crystallization temperature (T_{cc}), normalized cold crystallization enthalpy (ΔH_{cc}), melting temperature (T_m), and normalized enthalpy of melting (ΔH_m) were obtained from the heating scan while the crystallization temperature from the melt

(T_c) and normalized enthalpy of crystallization (ΔH_c) were determined from the cooling scan. The percentage of crystallinity (X_c) was determined using the following equation:

$$X_C = \left[\frac{\Delta H_m - \Delta H_{cc}}{\Delta H_m^0}\right] \cdot 100 \qquad (1)$$

Where ΔH_m^0 (J/g) represents the theoretical melt enthalpy of a fully crystalline bio-PA, considering 197 J/g for PA610 [28], 244 J/g for PA1010 [29] and 209.2 J/g for PA1012 [30]. Thermal stability was determined by thermogravimetric analysis (TGA) in a TGA/SDTA 851 thermobalance from Mettler-Toledo, LLC (Columbus, OH, USA). The heating program was set from 30 to 700°C at a heating rate of 20 °C /min in air atmosphere with a constant flow-rate of 66 mL/min. Approximately 5-7 mg of tube sample was used for the measurements. The onset degradation temperature was defined as the temperature at 5% weight loss ($T_{5\%}$) and the degradation temperature (T_{deg}) was obtained from the maximum value of the first derivative.

2.5. Thermomechanical characterization

Dynamic mechanical thermal analysis (DMTA) was conducted in tension mode using a DMA-1 from Mettler-Toledo GmbH (Greifensee, Switzerland). Tube samples of 5 mm were cut longitudinally into stripes (10x5x1 mm^3) and subjected to a temperature program ranging from 0 to 140°C at a heating rate of 2 °C/min, a deformation frequency of 1 Hz, and a strain of 0.1%. Vicat softening temperature and heat deflection temperature (HDT) were measured in a Vicat/HDT station VHDT 20 from Metrotec S.A. (San Sebastián, Spain). Vicat values were obtained according ISO 306, following B50 method. This was performed on circular compression-molded samples with a diameter of 2.5 cm and a thickness of 4 mm prepared in a 10-Tn hydraulic press from Robima S.A. (Valencia, Spain) equipped with two hot aluminum plates and a temperature controller from Dupra S.A. (Castalla, Spain) [31].Specimens were cut using a die on a hydraulic press model MEGA KCK-15A from Melchor Gabilondo S.A. (Vizcaya, Spain) [32]. During this test, each specimen was placed in the testing apparatus so that the penetrating needle rested on its surface at least 1 mm from the edge. The applied force was 50 N and the heating rate was 50 °C/h.

Regarding HDT characterization, this was carried out using 80-mm long tubes based on ISO 75. The bio-PA tubes were placed at a distance between supporting edges of 60 mm and a weight of 320 g was applied, which corresponds to a pressure of 1.8 MPa. The heating rate was 120 °C/h as recommended in the corresponding standard.

Dimensional stability was studied by measuring the coefficient of linear expansion (CLTE) using a thermomechanical analyzer (TMA) Q400 model from TA Instruments (Delaware, USA). Test was performed on 7-mm long tubes. The heating program was set from 0 to 140°C with a constant heating rate of 2 °C/min and a load of 0.02 N. All measurements were done in triplicate.

2.6. Mechanical characterization

Tube specimens with a total length of 150 mm were tested in a universal test machine ELIB 30 from S.A.E. Ibertest (Madrid, Spain). Tensile tests were performed according to ISO 527. A 5-kN load cell and a cross-head speed of 5 mm/min were employed. Shore D hardness was determined in a durometer 676-D model from J. Bot S.A. (Barcelona, Spain) following ISO 868. All specimens were tested in a controlled chamber at room conditions, *i.e.* 23°C and 50% RH. At least six samples for each material were analyzed and averaged.

2.7. Water uptake measurements

Tube specimens of 80 mm were immersed in distilled water at 23 ± 1°C. Samples were extracted weekly and weighed in an analytical balance with an accuracy of ± 0.1 mg after removing the residual water with a dry cloth. The evolution of water uptake was followed over a whole period of 9 weeks. Measurements were done in triplicate.

3. Results and discussion

3.1. Visual aspect

Figure 3 shows the resultant profile-extruded tubes of the here-studied bio-PAs. One can observe in this image that continuous tubes with an OD of 10mm and a homogenous surface were produced. In general, the obtained bio-PA tubes presented high translucency but low

transparency, as expected for semi-crystalline polymers. No visual differences among the tubes were noticeable.

3.2. Chemical properties

Figure 4 shows the FTIR characteristic absorption peaks of the here-studied bio-based PAs. The broad absorption peak at ~3300 cm^{-1} has been mainly reported for the valence stretch vibrations of hydrogen atoms bonded as N–H of terminal amine groups [33-35]. The intense peaks observed at 2919 and 2851 cm^{-1} are caused from the asymmetric and symmetric C–H stretching vibration of methylene groups, respectively [28]. These peaks were very similar for the three bio-PAs. However, some interesting changes can be observed in these spectra at lower wavenumbers.

For the PA1012 and PA1010 the main absorption peak was seen at 1635 cm^{-1}, which has been well assigned to the C=O of Amide I in both α- and β-crystalline phases [29, 34, 35]. This moved down to 1632 cm^{-1} in the case of PA610, which can be either related to its higher amide density or changes in crystallinity. In addition, the strong peak at 1540 cm^{-1} in the spectra of both PA1012 and PA610, which belongs to the bending vibration of N–H in Amide II [34-36], shifted to 1535 cm^{-1} for PA1010. This band displacement to a lower frequency region has recently been ascribed to crystallization increases in polyamides [37]. The band at 1462 cm^{-1} has been related to the contribution of the C–N stretching vibration of amide groups [29] and C–H bending vibration in methylene groups [35]. The group of bands in the range 1300-1200 cm^{-1} are attributed to the gauche nitrogen-methylene group, *i.e.* N–H and C–H twisting [28, 38]. These absorption bands, showing a main peak centered at 1238 cm^{-1}, became sharper and more intense in the spectrum of PA1010. This suggests that chain conformation of the methylene sequences in PA1010 was more ordered. The aforementioned changes can be therefore ascribed to the more symmetrical chain structure of PA1010, which favors molecular folding and subsequent crystallization. The low-intense bands at 1160 and 940 cm^{-1} that can be observed for both PA1010 and PA1012 are attributed to the skeletal motion and in-plane modes of CO–NH bonds, respectively, which are characteristic of amide groups in semi-crystalline polyamides

247 [39]. For PA610, this peak shifted towards 922 cm^{-1}. In this sense, the bands located at 936 and
248 922 cm^{-1} have been attributed to the amide C–C=O vibration stretching that are related to the
249 crystalline and amorphous phases in PA66, respectively [28]. This indicates that the structure of
250 PA610 was predominantly amorphous. Finally, the peak at 720 cm^{-1} corresponds to the shear
251 vibration of methylene groups, *i.e.* C–H rocking [35]. This was more intense in the spectra of
252 PA1012 and PA1010 than in the PA610 spectrum possibly due to its lower CH_2/CONH ratio.

253 ***3.3. Thermal properties***

254 **Figure 5** includes the heating and cooling DSC scans of the bio-PA tubes and the results
255 obtained from these curves are summarized in **Table 1**. The melting thermograms, gathered in
256 **Figure 5a**, show that all bio-PAs showed T_g values in the range of 40-60°C. However, these
257 were difficult to elucidate, particularly for PA1010 and PA1012, probably due to their reduced
258 amorphous phase. It can also be observed that the bio-PA tubes did not show any cold
259 crystallization peak before melting, which can be related to the efficient cooling conditions and
260 annealing treatment performed in the last stage of profile extrusion.
261 All three bio-PAs presented one intense melting peak, suggesting the presence of a predominant
262 single crystalline form in the tubes that can be ascribed to the slow cooling rate applied during
263 profile extrusion. This observation differentiates the here-evaluated bio-PAs from short-chain
264 polyamides (*e.g.* PA6) that typically exhibit a polymorphism behavior, showing multiple
265 melting peaks of different intensities due to the presence of different crystalline forms where
266 distinct crystalline lamellae coexist, *i.e.* α, β, and γ [40]. In particular, the α-form is the most
267 stable and perfect crystalline phase, in which hydrogen bonds are formed between antiparallel
268 chains, stretching to a lower extent the rotation of the polymer chains and, therefore, increasing
269 chains packing [41]. However, one can also observe that the melting peaks were relatively
270 broad, showing the presence of a shoulder at lower temperatures. This was particularly
271 noticeable for PA610, which can denote the presence of an additional crystallite population.
272 According to Thompson-Gibbs relationship, this reflects the melt recrystallization of less

perfect crystals, which has been well reported for either conventional polyamides (*e.g.* PA6, PA66) [42, 43] but also for newly PA610 [36] and PA1010 [44].

Due to its lower CH_2/CONH ratio, PA610 presented the highest value of T_m (~215°C) while PA1010 and PA1012 melted at approximately 195 and 183°C, respectively. Therefore, the here-studied bio-PAs followed perfectly correlation between melting temperature and CH_2/CONH ratio. For instance, a similar melting point for PA1012 has been recently reported [45]. Regarding PA1010, this melting point has been precisely ascribed to the above-described α-form crystals, which are based on a triclinic system [44]. This value certainly places the thermal properties of these bio-PAs in between those of conventional medium- or long-chain PA12 (~179°C) [46] and short-chain PA6 (~221°C) [47]. Furthermore, as commented above, the melting peaks of PA1010 and PA1012 were clearly sharper than that of PA610.

Figure 5b shows the DSC thermograms taken during the cooling scan. All bio-PAs crystallized from the melt in a single peak according to their CH_2/CONH ratio too. In particular, values of T_c were observed at 182, 177, and 163°C for PA610, PA1010, and PA1012, respectively. It can be observed that PA1010 presented the highest X_c value (~27%) while PA610 showed the lowest (~8%), even though the latter is based on a shorter chain structure, *i.e.* its amide density per chain is higher [24]. The larger crystallinity degree observed for PA1010 can be related to its more symmetrical chain structure in which the diamine and dicarboxylic acid are both based on a C10 chemical structure. This can potentially result in a high regular spacing of the amide groups along the polymer chains that, in turns, favors the formation of orderly regions of crystallinity. In relation to the crystallinity degree observed for PA1012 (~16%), which was higher than PA610 but lower than PA1010, this can be explained by a decrease in the average number of inter-chain hydrogen bonds caused by the increase of the diacid chain length [28].

Table 1 also includes thermal stability values of the profile-extruded bio-PA tubes. All samples presented similar values of thermal degradation. No moisture content was observed in the samples since any noticeable weight loss was observed below 100°C. In particular, the bio-PA tubes remained stable up to approximately 320-340°C, showing a T_{deg} of *ca.* 460°C. Similar thermal degradation profiles in bio-PAs have been previously reported [44, 48]. It was

301 particularly indicated that this mainly involves a β−C−H transfer reaction mechanism,
302 producing ketoamides as the primary decomposition products [49].

303 ***3.4. Thermomechanical properties***

304 **Figure 6** presents the temperature dependence of the storage modulus (G') and damping factor
305 (tan δ) of the bio-PA tubes. It can be clearly observed in **Figure 6a** that, as temperature
306 increased, the storage modulus gradually decreased. At the glassy plateau region, for instance
307 25°C, PA610 displayed higher storage modulus (~1225 MPa) than PA1010 (~1030 MPa) and,
308 more significantly, than PA 1012 (~618 MPa). This value was expected due to the lower
309 CH_2/CONH ratio of PA610. However, comparison of the biopolymer tubes in the rubbery
310 plateau region, for instance 100°C, indicated that the storage modulus of PA1010 was
311 considerably higher (~259 MPa) than that observed for both PA1012 (~164 MPa) and PA610
312 (~107 MPa). This interesting observation confirms previous chemical and thermal analyses,
313 indicating that PA610 is a highly amorphous material. As a result, in the rubber-like state, *i.e.*
314 above T_g, mechanical strength of PA610 was considerably reduced. On the contrary, the higher
315 crystallinity of PA1012 and, particularly, of PA1010, potentially restricted the movement of the
316 polymer chains and improved elasticity as temperature is increased.
317 **Figure 6b** shows the damping factor as a function of temperature for the PA610, PA1010, and
318 PA1012 tubes measured by DMTA. A loss peak can be seen in the curves that points out the α-
319 relaxation of the bio-PAs, which is related to their T_g. Due to PA610 presents the lowest
320 CH_2/CONH ratio, *i.e.* the highest amide density, this bio-PA exhibited the highest α-relaxation
321 value (~51 °C). This was followed by PA1010 (~38°C) and PA1012 (~27°C). Therefore, the α-
322 relaxation values perfectly correlated with the CH_2/CONH ratio. In addition, the peak intensities
323 for both PA1010 and PA1012 did not only shift towards lower temperatures but, more
324 importantly, these were also significantly lower than that for PA610. This observation clearly
325 confirms that a lower amount of amorphous part underwent glass transition in both PA1010 and
326 PA1012 when compared to PA610.

Table 2 includes the coefficients of linear thermal expansion (CLTE) of the bio-PA tubes below and above T_g. All samples showed lower CLTE values below T_g than above T_g. By increasing temperature, the bio-PA tubes offered less resistance against thermal expansion, leading higher CLTE values. The highest CLTE values were clearly observed for PA1010, which is related to the formation of a stronger crystal network that certainly reduces the biopolymer degree of freedom. Similar values were recently reported for compression-molded PA610 parts [48]. From the thermal expansion test, T_g values were also obtained, defined as the temperature in which the slope of CLTE changes. As one can observe in the table, these values ranged from 40-50°C, following the same trend as the α-relaxation values determined above by DMTA. In general, all bio-PAs presented T_g values close to that of PA6 (~53°C) [47]. Indeed, variations in the aliphatic chain length within the repeating unit are known to have a small effect on T_g of short- and medium-chain polyamides [50].

In **Table 2** the values of Vicat softening point and HDT are also listed. These are two important factors when selecting a plastic material for a high-temperature application. In this regard, Vicat reflects the softening degree that would be reached when the bio-PAs are subjected to indentation conditions at a given temperature. In relation to HDT, it determines their upper mechanical use in terms of the temperature limit. In this table, it can be observed that, while PA1010 presented the highest values of both thermomechanical factors, the lowest values were observed for PA610. From the above discussion, these results can be certainly ascribed to the degree of crystallinity observed for the different bio-PAs, showing a good correlation with previous DMTA results. In particular, the here-obtained HDT value for the PA1010 tubes (~60°C) is positively close to that previously reported for injection-molded pieces of PA6 (62°C) [51].

3.5. Mechanical properties

Figure 7 shows the typical tensile stress-strain curves at room temperature for the bio-PA tubes. The mechanical results, in terms of tensile modulus (E), tensile strength at yield (σ_y), and elongation at break (ε_b), are summarized in **Table 3**. The mechanical curve of PA610 showed a

double yielding while the PA1010 and PA1012 curves displayed a more pronounced ductile behavior. Interestingly, all tensile curves presented strain-hardening phenomenon at large strains. This has been well explained in semi-crystalline polyamides by an induced mechanism of crystals lamellae reorientation process or, in some cases, by a change of both crystal form and size during plastic deformation [52, 53]. The tensile moduli were obtained from the initial linear regions of the curves in the lower strain range, *i.e.* <0.025%. As it was previously observed during DMTA, PA610 showed the highest tensile modulus, *i.e.* 516.8 MPa. This was very similar to that of PA1010, *i.e.* 507.4 MPa, but higher than that of PA1012, *i.e.* 408.6 MPa. However, in relation to tensile strength, the PA1010 tube presented the highest value, *i.e.* ~40 MPa, which was approximately 14% and 28% higher than those observed for PA1012 and PA610, respectively. As previously described during the thermomechanical analysis, the enhanced mechanical strength of PA1010 in comparison to the other bio-PA tubes can be ascribed to its higher degree of crystallinity. Furthermore, PA1012 produced the most flexible tubes, showing an elongation-at-break value of approximately 245% due to this bio-PA presents the highest methylene content [54]. Regarding the ductility of the other tubes, PA1010 showed a slightly higher value of elongation at break than PA610, *i.e.* 197% *vs.* 186%. It is also worthy to note that the here-studied bio-PA tubes presented intermediate elongation-at-break values between those observed for more elastic PA6 (140%) [55] and more ductile PA12 (286%) [56], both processed by injection molding.

Finally, in **Table 3** the values of Shore D hardness are also included. One can observe that hardness followed the same trend previously observed in the tensile modulus, having the PA610 and PA1010 tubes the highest values. Thus, higher values of hardness can be related to an enhancement of the biopolymer elasticity [57]. However, differences in hardness among the bio-PA tubes were relatively small. In summary, from a mechanical point of view, it can be concluded that PA1010 certainly offers enhanced flexibility with the additional benefit of a relatively high mechanical strength and hardness.

3.6. Water Uptake

Water absorption is one of the most important characteristics of polyamide-based parts for plastics engineering applications. In particular, this phenomenon has been widely studied for polyamides, indicating that water molecules are sorbed only in the amorphous regions by involving two neighboring amide groups in an accessible region [58]. In the first amide, a water molecule is bound by dipole-dipole interactions to the carbonyl groups, *i.e.* hydrogen bonds, while two other water molecules remain loosely bonded in the other amide between the C–O and N–H groups [49]. As it can be observed in **Figure 8**, the immersed bio-PA tubes absorbed different weight amounts of water until these reached a *plateau* after approximately 4 weeks. In particular, water absorption values of 1.93, 1.20, and 0.95 wt.-% were observed for PA610, PA1010, and PA1012, respectively. Therefore, as it has been already established in previous studies concerning polyamides [59], an increase in the CH_2/CONH ratio resulted in a decrease in the water uptake at equilibrium. However, since water is known to be only absorbed by the amorphous phase, crystallinity had a noticeable effect on water uptake too. This explains the significant difference observed between PA610, more amorphous, and the other two bio-PAs. In particular, it is considered that polymer crystallites can hinder translational mobility of water molecules that are sorbed in the amorphous phase [60]. Overall, the water absorption of the here-developed bio-PA tubes was relatively low, in particular when these values are compared to that of conventional PA6 (~8.5 wt.-%) [61]. This encouragingly suggests that their mechanical properties would be scarcely affected by atmospheric humidity.

4. Conclusions

The present study ruled out the differences in the thermal, thermomechanical, and mechanical properties and water uptake of profile-extruded tubes of PA610, PA1010, and PA1012. The obtained data were analyzed and compared in view of their different chemical structures and degrees of crystallinity. It was observed that the CH_2/CONH ratio had a main role in determining the thermal properties, *i.e.* T_g, T_c, and T_m, and water uptake, but it had a lower impact on the thermomechanical and mechanical performance than their crystallinity degree. In particular, it was observed that the PA610 tubes presented a similar thermal performance but

lower thermomechanical and mechanical properties than short-chain polyamides, for instance PA6, being relatively rigid at room temperature. Meanwhile, PA1010 interestingly produced semi-crystalline tubes with very balanced physical properties, showing peculiar properties of an engineering thermoplastic. Finally, the PA1012 tubes were much more flexible and these may find applications in the same domain as, for instance, those made of PA12. In general, the PA1010 and PA1012 chemical structures have longer aliphatic segments and lower amide densities than PA610, but these still show higher melting transition temperature than general-purpose plastics such as polyolefins. Therefore, these novel bio-PA tubes can be a good candidate for engineering applications with enhanced sustainable characteristics. Additionally, the effect of chemical agents, fuels, and industrial fluids on the stability and performance of these bio-based polyamide tubes would warrant further investigation.

Acknowledgements

This research was supported by the Ministry of Economy and Competitiveness (MINECO) program number MAT2014-59242-C2-1-R and AGL2015-63855-C2-1-R and Generalitat Valenciana (GV) program number GV/2014/008. Quiles-Carrillo wants to thank GV for financial support through a FPI grant (ACIF/2016/182) and the Spanish Ministry of Education, Culture, and Sports (MECD) for his FPU grant (FPU15/03812).

References

[1] K. Marchildon, Polyamides – Still Strong After Seventy Years, Macromolecular Reaction Engineering, 5 (2011) 22-54.

[2] W.H. Carothers, Studies on polymerization and ring formation. I. An introduction to the general theory of condensation polymers, Journal of the American Chemical Society, 51 (1929) 2548-2559.

[3] M. Pervaiz, M. Faruq, M. Jawaid, M. Sain, Polyamides: Developments and applications towards next-generation engineered plastics, Current Organic Synthesis, 14 (2017) 146-155.

[4] M. Fischer, Polyamides (PA), Kunststoffe Plast Europe, 94 (2004) 90-95.

[5] V. Siejak, H.B. Lüchtefeld, Global market for high-tenacity polyamide and polyester filament yams 2008-2010, Chemical Fibers International, 61 (2011) 135-136.

[6] T.M. Carole, J. Pellegrino, M.D. Paster, Opportunities in the industrial biobased products industry, Applied Biochemistry and Biotechnology - Part A Enzyme Engineering and Biotechnology, 115 (2004) 871-885.

[7] A. Nakayama, Development of biobased polyamides, Sen'i Gakkaishi, 66 (2010) 368-372.

[8] L. Shen, E. Worrell, M. Patel, Present and future development in plastics from biomass, Biofuels, Bioproducts and Biorefining, 4 (2010) 25-40.

[9] F. Pardal, S. Salhi, B. Rousseau, M. Tessier, S. Claude, A. Fradet, Unsaturated Polyamides from Bio-Based Z-octadec-9-enedioic Acid, Macromolecular Chemistry and Physics, 209 (2008) 64-74.

[10] D.S. Ogunniyi, Castor oil: A vital industrial raw material, Bioresource Technology, 97 (2006) 1086-1091.

[11] M. Desroches, M. Escouvois, R. Auvergne, S. Caillol, B. Boutevin, From Vegetable Oils to Polyurethanes: Synthetic Routes to Polyols and Main Industrial Products, Polymer Reviews, 52 (2012) 38-79.

[12] S. Olsnes, The history of ricin, abrin and related toxins, Toxicon, 44 (2004) 361-370.

[13] A.E. Koigeldina, T. Nurgasenov, B.S. Rahmetolaevich, Structure of a crop and productivity of a castor-oil plant depending on periods of sowing, norms of sowing and seeding depth, Biosciences Biotechnology Research Asia, 12 (2015) 51-57.

[14] L.S. Severino, D.L. Auld, M. Baldanzi, M.J.D. Cândido, G. Chen, W. Crosby, D. Tan, X. He, P. Lakshmamma, C. Lavanya, O.L.T. Machado, T. Mielke, M. Milani, T.D. Miller, J.B. Morris, S.A. Morse, A.A. Navas, D.J. Soares, V. Sofiatti, M.L. Wang, M.D. Zanotto, H. Zieler, A review on the challenges for increased production of castor, Agronomy Journal, 104 (2012) 853-880.

[15] Y. Jiang, K. Loos, Enzymatic synthesis of biobased polyesters and polyamides, Polymers, 8 (2016).

[16] M. Yasuda, A. Miyabo, Polyamide derived from castor oil, Sen'i Gakkaishi, 66 (2010) P137-P142.

[17] A.K. Vasishtha, R.K. Trivedi, G. Das, Sebacic acid and 2-octanol from castor oil, Journal of the American Oil Chemists' Society, 67 (1990) 333-337.

[18] E.O. Ogunsona, M. Misra, A.K. Mohanty, Sustainable biocomposites from biobased polyamide 6,10 and biocarbon from pyrolyzed miscanthus fibers, Journal of Applied Polymer Science, 134 (2017) n/a-n/a.

[19] M. Winnacker, B. Rieger, Biobased Polyamides: Recent Advances in Basic and Applied Research, Macromolecular Rapid Communications, 37 (2016) 1391-1413.

[20] M. Niaounakis, Biopolymers: Processing and Products, William Andrew Publishing, Oxford, 2015.

[21] N.A. Jones, E.D.T. Atkins, M.J. Hill, S.J. Cooper, L. Franco, Chain-folded lamellar crystals of aliphatic polyamides. Investigation of nylons 4 8, 4 10, 4 12, 6 10, 6 12, 6 18 and 8 12, Polymer, 38 (1997) 2689-2699.

[22] J.J. Rajesh, J. Bijwe, U. Tewari, Abrasive wear performance of various polyamides, Wear, 252 (2002) 769-776.

[23] J. John Rajesh, J. Bijwe, B. Venkataraman, U.S. Tewari, Effect of impinging velocity on the erosive wear behaviour of polyamides, Tribology International, 37 (2004) 219-226.

[24] P. Adriaensens, A. Pollaris, R. Rulkens, V.M. Litvinov, J. Gelan, Study of the water uptake of polyamide 46 based copolymers by magnetic resonance imaging relaxometry, Polymer, 45 (2004) 2465-2473.
[25] H.F. Giles Jr, J.R. Wagner Jr, E.M. Mount Iii, 50 - Pipe and Tubing Extrusion, Extrusion, William Andrew Publishing, Norwich, NY, 2005, pp. 487-496.
[26] J. Vlachopoulos, D. Strutt, Polymer processing, Materials Science and Technology, 19 (2003) 1161-1169.
[27] J. Vlachopoulos, D. Strutt, The SPE Guide on Extrusion Technology and Troubleshooting, Society of Plastics Engineers, Brookfield, CT, 2001.
[28] T. Elzein, M. Brogly, J. Schultz, Crystallinity measurements of polyamides adsorbed as thin films, Polymer, 43 (2002) 4811-4822.
[29] M. Yan, H. Yang, Improvement of polyamide 1010 with silica nanospheres via in situ melt polycondensation, Polymer Composites, 33 (2012) 1770-1776.
[30] S. Gogolewski, K. Czerntawska, M. Gastorek, Effect of annealing on thermal properties and crystalline structure of polyamides. Nylon 12 (polylaurolactam), Colloid and Polymer Science Kolloid Zeitschrift & Zeitschrift für Polymere, 258 (1980) 1130-1136.
[31] S. Torres-Giner, N. Montanes, V. Fombuena, T. Boronat, L. Sanchez-Nacher, Preparation and characterization of compression-molded green composite sheets made of poly(3-hydroxybutyrate) reinforced with long pita fibers, Advances in Polymer Technology, (2017) DOI: 10.1002/adv.21789.
[32] S. Torres-Giner, N. Montanes, O. Fenollar, D. García-Sanoguera, R. Balart, Development and optimization of renewable vinyl plastisol/wood flour composites exposed to ultraviolet radiation, Materials & Design, 108 (2016) 648-658.
[33] W. Kong, K. Hu, X. Fu, D. Guo, J. Lei, Preparation and Characterization of Thermoplastic Elastomer Based on Amino-terminated Polyamide-6 and Diisocyanate-terminated Polytetramethylene Glycol, Polymer-Plastics Technology and Engineering, 55 (2016) 1-8.
[34] H. Li, Z. Li, The effect of reactive compatibilization of carboxylated polystyrene on morphology and toughness of polyamide-1010/polystyrene blends, Polymer International, 48 (1999) 124-128.
[35] M. Porubská, O. Szöllős, A. Kóňová, I. Janigová, M. Jašková, K. Jomová, I. Chodák, FTIR spectroscopy study of polyamide-6 irradiated by electron and proton beams, Polymer Degradation and Stability, 97 (2012) 523-531.
[36] F.-C. Pai, S.-M. Lai, H.-H. Chu, Characterization and Properties of Reactive Poly(lactic acid)/Polyamide 610 Biomass Blends, Journal of Applied Polymer Science, 130 (2013) 2563-2571.
[37] C. Wan, F. Zhao, X. Bao, B. Kandasubramanian, M. Duggan, Effect of POSS on crystalline transitions and physical properties of polyamide 12, Journal of Polymer Science Part B: Polymer Physics, 47 (2009) 121-129.
[38] S. Rhee, J.L. White, Investigation of structure development in polyamide 11 and polyamide 12 tubular film extrusion, Polymer Engineering & Science, 42 (2002) 134-145.
[39] N. Vasanthan, D.R. Salem, FTIR spectroscopic characterization of structural changes in polyamide-6 fibers during annealing and drawing, Journal of Polymer Science Part B: Polymer Physics, 39 (2001) 536-547.
[40] E. Logakis, C. Pandis, V. Peoglos, P. Pissis, C. Stergiou, J. Pionteck, P. Pötschke, M. Mičušík, M. Omastová, Structure–property relationships in polyamide 6/multi-walled carbon nanotubes nanocomposites, Journal of Polymer Science Part B: Polymer Physics, 47 (2009) 764-774.
[41] J. Jiang, D. Zhang, Y. Zhang, K. Zhang, G. Wu, Influences of Carbon Nanotube Networking on the Conductive, Crystallization, and Thermal Expansion Behaviors of PA610-Based Nanocomposites, Journal of Macromolecular Science, Part B, 52 (2013) 910-923.
[42] J.P. Bell, P.E. Slade, J.H. Dumbleton, Multiple melting in nylon 66, Journal of Polymer Science Part A-2: Polymer Physics, 6 (1968) 1773-1781.
[43] Q.-X. Zhang, Z.-Z. Yu, M. Yang, J. Ma, Y.-W. Mai, Multiple melting and crystallization of nylon-66/montmorillonite nanocomposites, Journal of Polymer Science Part B: Polymer Physics, 41 (2003) 2861-2869.

[44] F. Xiuwei, L. Xiaohong, Y. Laigui, Z. Zhijun, Effect of in situ surface-modified nano-SiO2 on the thermal and mechanical properties and crystallization behavior of nylon 1010, Journal of Applied Polymer Science, 115 (2010) 3339-3347.
[45] J. Song, J. Liu, Y. Zhang, L. Chen, Y. Zhong, W. Yang, Basalt fibre-reinforced PA1012 composites: Morphology, mechanical properties, crystallization behaviours, structure and water contact angle, Journal of Composite Materials, 49 (2014) 415-424.
[46] C. Yan, L. Hao, L. Xu, Y. Shi, Preparation, characterisation and processing of carbon fibre/polyamide-12 composites for selective laser sintering, Composites Science and Technology, 71 (2011) 1834-1841.
[47] J.W. Cho, D.R. Paul, Nylon 6 nanocomposites by melt compounding, Polymer, 42 (2001) 1083-1094.
[48] S. Ghaffari Mosanenzadeh, M.W. Liu, A. Osia, H.E. Naguib, Thermal Composites of Biobased Polyamide with Boron Nitride Micro Networks, Journal of Polymers and the Environment, 23 (2015) 566-579.
[49] E.C. Botelho, M.C. Rezende, Monitoring of Carbon Fiber/Polyamide Composites Processing by Rheological and Thermal Analyses, Polymer-Plastics Technology and Engineering, 45 (2006) 61-69.
[50] D.C. Prevorsek, R.H. Butler, H.K. Reimschuessel, Mechanical relaxations in polyamides, Journal of Polymer Science Part A-2: Polymer Physics, 9 (1971) 867-886.
[51] S. Xie, S. Zhang, F. Wang, M. Yang, R. Séguéla, J.-M. Lefebvre, Preparation, structure and thermomechanical properties of nylon-6 nanocomposites with lamella-type and fiber-type sepiolite, Composites Science and Technology, 67 (2007) 2334-2341.
[52] G.-F. Shan, W. Yang, B.-h. Xie, Z.-m. Li, J. Chen, M.-b. Yang, Double yielding behaviors of polyamide 6 and glass bead filled polyamide 6 composites, Polymer Testing, 24 (2005) 704-711.
[53] G.-F. Shan, W. Yang, M.-b. Yang, B.-h. Xie, Z.-m. Li, J.-m. Feng, Effect of crystallinity level on the double yielding behavior of polyamide 6, Polymer Testing, 25 (2006) 452-459.
[54] J.J. Rajesh, J. Bijwe, Investigations on scratch behaviour of various polyamides, Wear, 259 (2005) 661-668.
[55] I. Isik-Gulsac, U. Yilmazer, G. Bayram, Mechanical and rheological properties, and morphology of polyamide-6/organoclay/elastomer nanocomposites, Journal of Applied Polymer Science, 125 (2012) 4060-4073.
[56] T.D. Fornes, D.R. Paul, Structure and Properties of Nanocomposites Based on Nylon-11 and -12 Compared with Those Based on Nylon-6, Macromolecules, 37 (2004) 7698-7709.
[57] S. Torres-Giner, N. Montanes, T. Boronat, L. Quiles-Carrillo, R. Balart, Melt grafting of sepiolite nanoclay onto poly(3-hydroxybutyrate-co-4-hydroxybutyrate) by reactive extrusion with multi-functional epoxy-based styrene-acrylic oligomer, European Polymer Journal, 84 (2016) 693-707.
[58] M.W.A. Paterson, J.R. White, Effect of water absorption on residual stresses in injection-moulded nylon 6,6, Journal of Materials Science, 27 (1992) 6229-6240.
[59] L.P. Razumovskii, V.S. Markin, G.Y. Zaikov, Sorption of water by aliphatic polyamides. Review, Polymer Science U.S.S.R., 27 (1985) 751-768.
[60] P. Adriaensens, A. Pollaris, R. Carleer, D. Vanderzande, J. Gelan, V.M. Litvinov, J. Tijssen, Quantitative magnetic resonance imaging study of water uptake by polyamide 4,6, Polymer, 42 (2001) 7943-7952.
[61] C. Jördens, S. Wietzke, M. Scheller, M. Koch, Investigation of the water absorption in polyamide and wood plastic composite by terahertz time-domain spectroscopy, Polymer Testing, 29 (2010) 209-215.

TABLES

Table 1. Thermal properties obtained from the differential scanning calorimetry (DSC) and thermogravimetric analysis (TGA) curves in terms of normalized enthalpy of crystallization (ΔH_c), crystallization temperature (T_c), normalized enthalpy of melting (ΔH_m), melting temperature (T_m), amount of crystallinity (X_c), degradation temperature at 5% of mass loss ($T_{5\%}$), degradation temperature (T_{deg}), mass loss at T_{deg}, and residual mass at 650°C for polyamide 610 (PA610), polyamide 1010 (PA1010), and polyamide 1012 (PA1012).

Tube sample	**DSC**					**TGA**			
	ΔH_c (J g^{-1})	T_c (°C)	ΔH_m (J g^{-1})	T_m (°C)	Xc (%)	$T_{5\%}$ (°C)	T_{deg} (°C)	Mass loss (%)	Residual mass (%)
PA610	22.51 ± 1.03	182.6 ± 1.1	15.24 ± 0.85	215.5 ± 1.2	7.8 ± 0.8	331.9± 1.5	462.4 ± 1.6	47.3 ± 0.9	0.62 ± 0.06
PA1010	30.77 ± 1.18	176.5 ± 0.9	65.91 ± 0.94	195.4 ± 0.9	27.1 ± 1.2	323.3 ± 1.9	460.7 ± 1.1	47.6 ± 1.3	0.09 ± 0.03
PA1012	25.56 ± 0.96	163.4 ± 0.6	33.59 ± 1.05	183.4 ± 1.1	16.1 ± 0.9	337.6 ± 2.4	463.9 ± 1.3	45.3 ± 1.1	0.21 ± 0.04

Table 2. Thermomechanical properties in terms of the coefficient of linear thermal expansion (CLTE) below and above glass transition temperature (T_g), Vicat softening point, and heat deflection temperature (HDT) for polyamide 610 (PA610), polyamide 1010 (PA1010), and polyamide 1012 (PA1012).

Tube sample	CLTE test			Vicat (°C)	HDT (°C)
	CLTE below T_g (μm/m°C)	CLTE above T_g (μm/m°C)	T_g (°C)		
PA610	124.6 ± 1.4	139.8 ± 1.9	49.8 ± 1.2	87.2 ± 1.1	49.2 ± 0.5
PA1010	171.3 ± 1.6	254.6 ± 1.5	45.2 ± 1.3	137.4 ± 1.2	59.9 ± 1.1
PA1012	120.6 ± 1.3	142.2 ± 1.4	42.9 ± 1.4	120.3 ± 1.4	54.5 ± 0.7

Table 3. Mechanical properties in terms of tensile modulus (E), tensile strength at yield (σ_y), elongation at break (ε_b), and Shore D hardness for polyamide 610 (PA610), polyamide 1010 (PA1010), and polyamide 1012 (PA1012).

Tube sample	**Tensile test**			**Shore D hardness**
	E (MPa)	**σ_y (MPa)**	**ε_b (%)**	
PA610	516.8 ± 12.1	28.7 ± 0.3	185.6 ± 12.3	64.8 ± 0.8
PA1010	507.4 ± 24.9	39.9 ± 1.3	196.7 ± 11.7	64.2 ± 0.9
PA1012	408.6 ± 15.1	34.3 ± 0.5	245.3 ± 14.4	61.6 ± 1.0

FIGURE CAPTIONS

Figure 1. Chemical structure and bio-based weight content of polyamide 610 (PA610), polyamide 1010 (PA1010), and polyamide 1012 (PA1012).

Figure 2. Schematic representation of the profile extrusion process.

Figure 3. Profile-extruded tubes of polyamide 610 (PA610), polyamide 1010 (PA1010), and polyamide 1012 (PA1012).

Figure 4. Fourier transform infrared (FTIR) spectra, from bottom to top, of polyamide 610 (PA610), polyamide 1010 (PA1010), and polyamide 1012 (PA1012). Arrows indicate the bands discussed in the text.

Figure 5. Differential scanning calorimetry (DSC) curves of polyamide 610 (PA610), polyamide 1010 (PA1010), and polyamide 1012 (PA1012) for: a) Heating scan; b) Cooling scan.

Figure 6. Dynamic mechanical thermal analysis (DMTA) curves of polyamide 610 (PA610), polyamide 1010 (PA1010), and polyamide 1012 (PA1012) for: a) Storage modulus *vs.* temperature; b) Damping factor (tan δ) *vs.* temperature.

Figure 7. Typical stress-strain curves of polyamide 610 (PA610), polyamide 1010 (PA1010), and polyamide 1012 (PA1012) tubes.

Figure 8. Water absorption of polyamide 610 (PA610), polyamide 1010 (PA1010), and polyamide 1012 (PA1012) tubes.

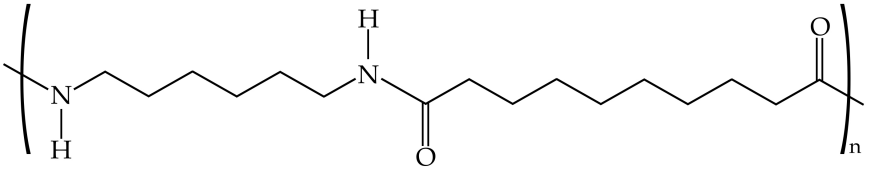

PA610

Based up to 63% on renewable raw materials

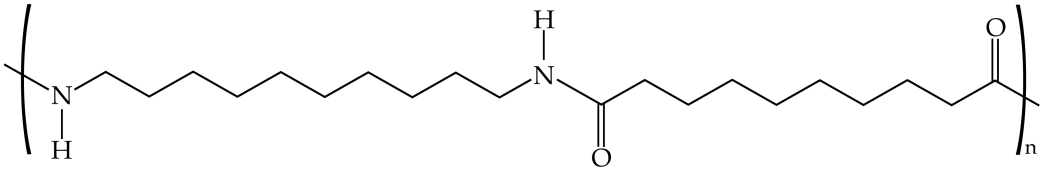

PA1010

Based up to 100% on renewable raw materials

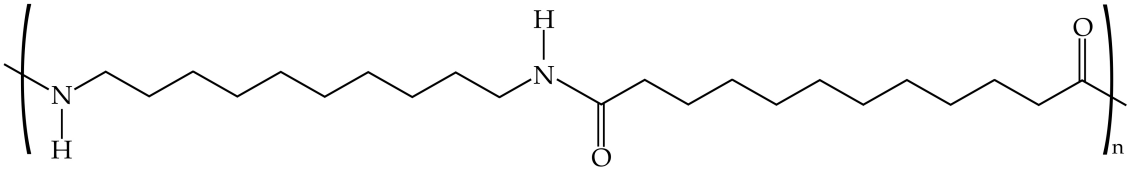

PA1012

Based from 45 to 100% on renewable raw materials

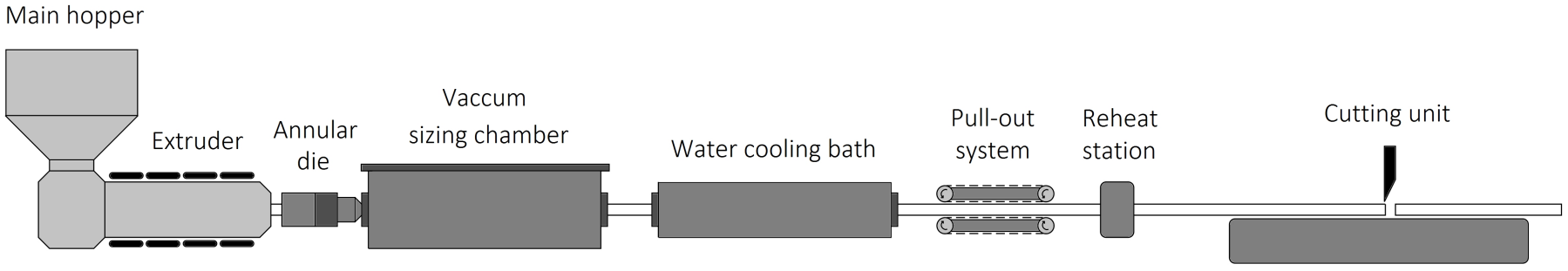
Main hopper
Extruder
Annular die
Vaccum sizing chamber
Water cooling bath
Pull-out system
Reheat station
Cutting unit

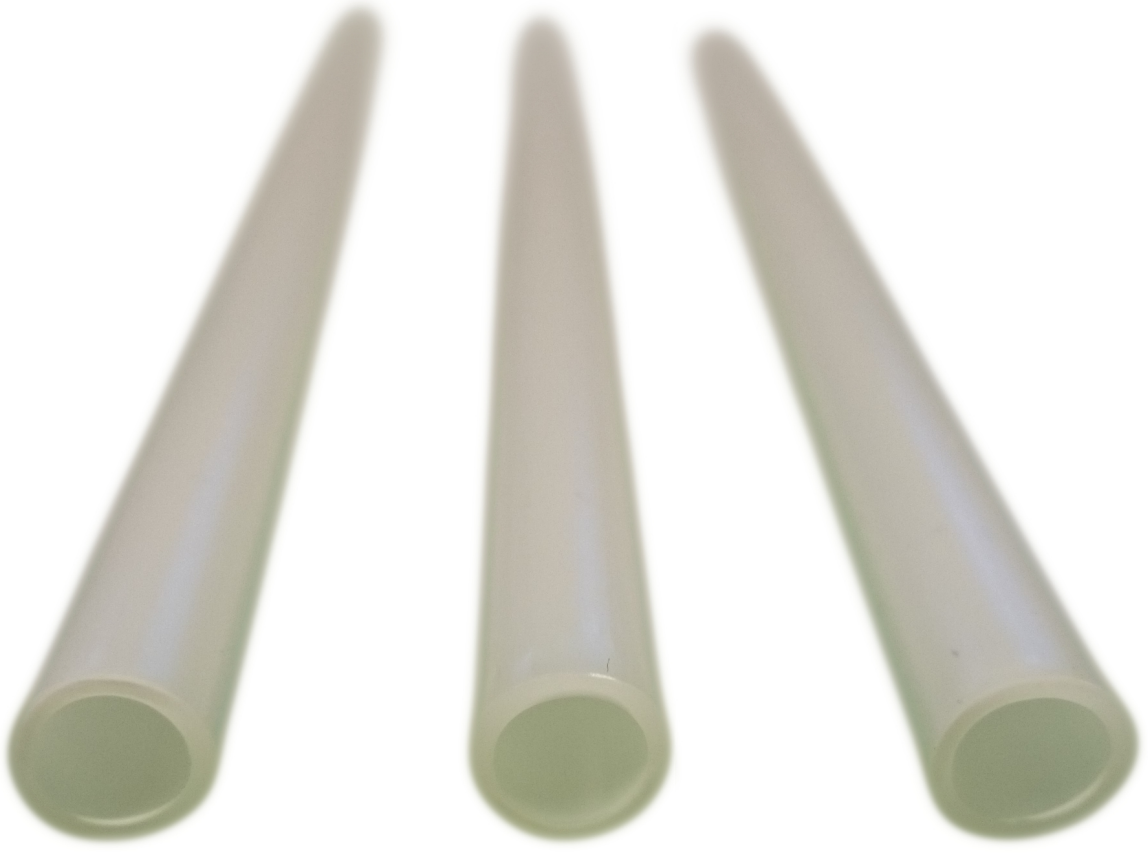

PA610 PA1010 PA1012

10 mm

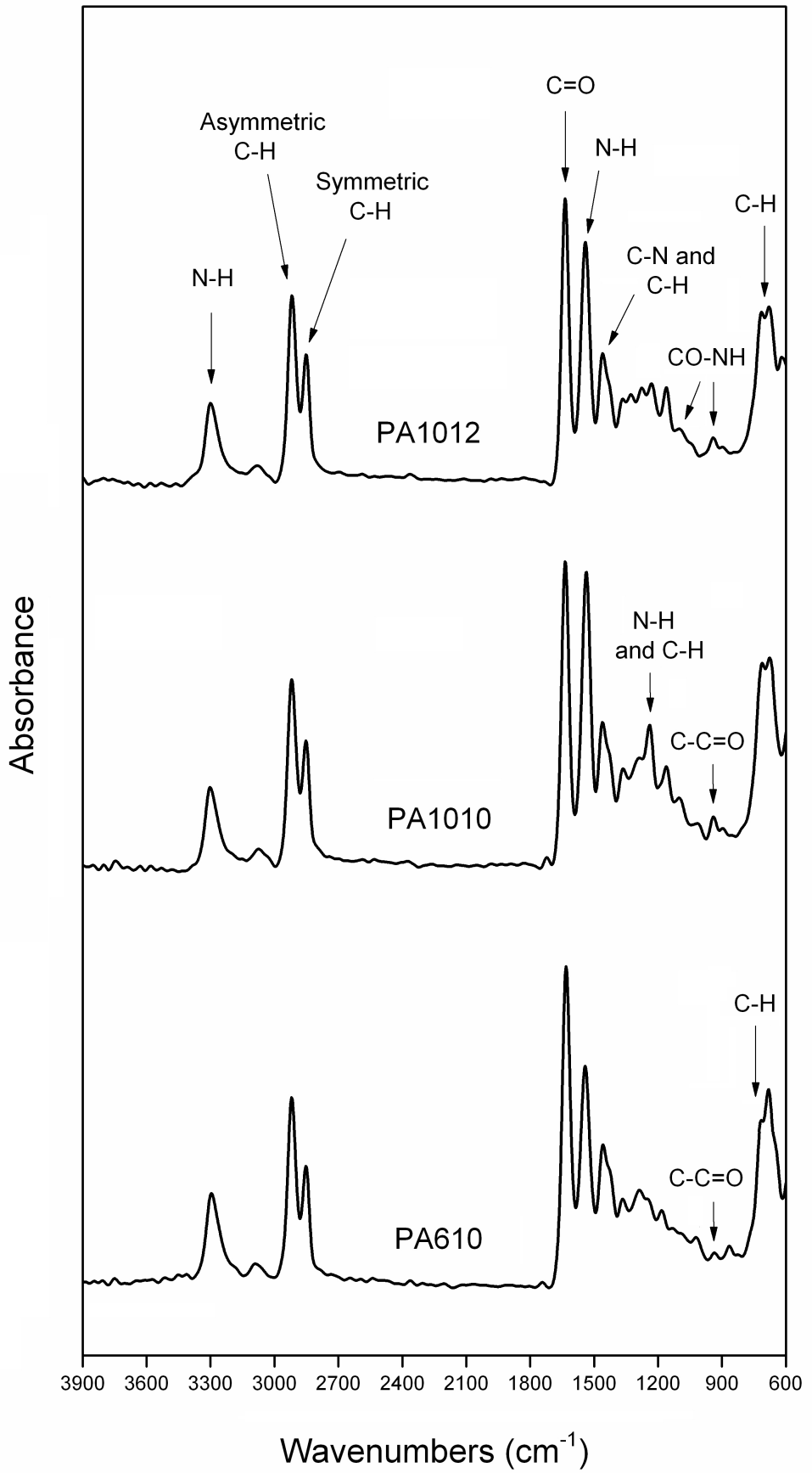
C=O
Asymmetric
C-H
N-H
Symmetric
C-H
C-H
N-H
C-N and
C-H
CO-NH
PA1012
N-H
and C-H
C-C=O
PA1010
C-H
C-C=O
PA610
Absorbance
3900 3600 3300 3000 2700 2400 2100 1800 1500 1200 900 600
Wavenumbers (cm-1)

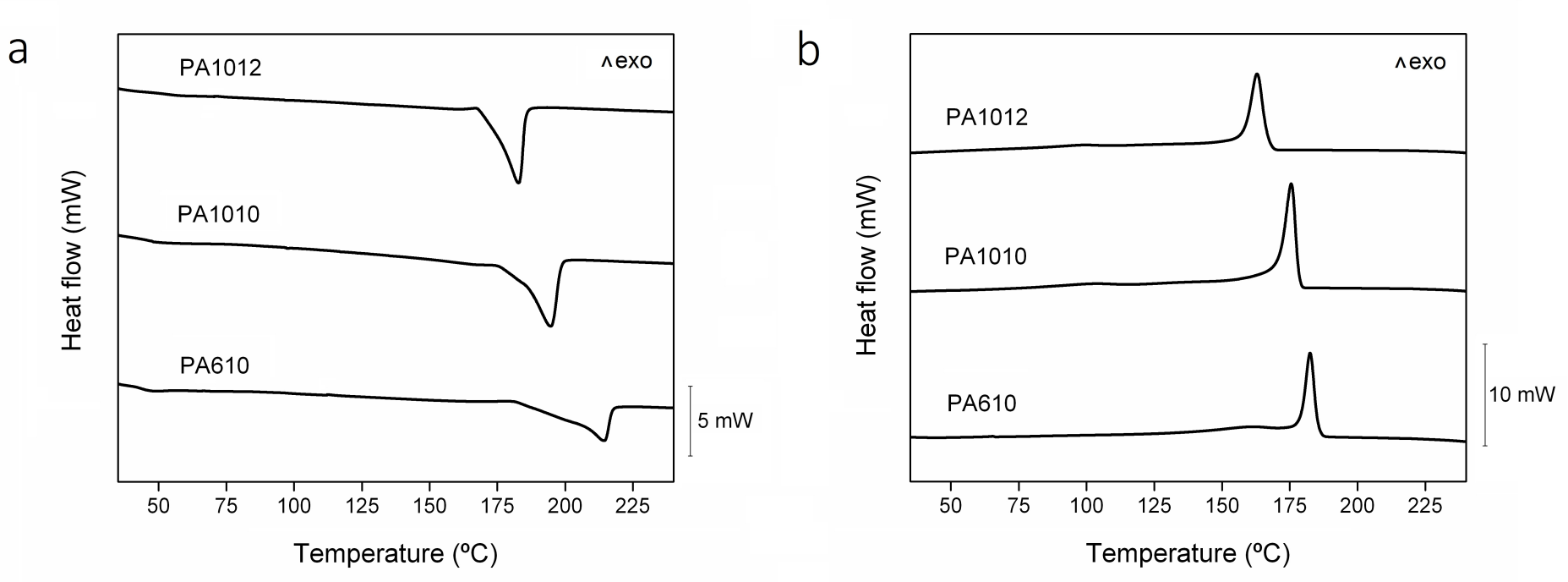
a
PA1012
^exo
PA1010
PA610
Heat flow (mW)
5 mW
50
75
100
125
150
175
200
225
Temperature (ºC)
b
PA1012
^exo
PA1010
PA610
Heat flow (mW)
10 mW
50
75
100
125
150
175
200
225
Temperature (ºC)

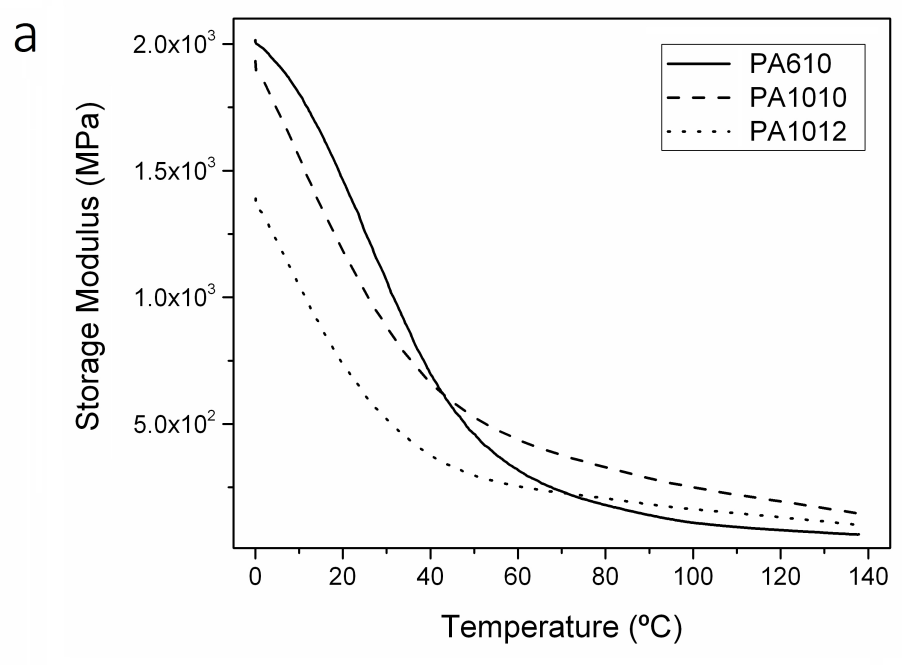
a
Storage Modulus (MPa)
2.0x10^3
1.5x10^3
1.0x10^3
5.0x10^2
0
20
40
60
80
100
120
140
Temperature (ºC)
PA610
PA1010
PA1012

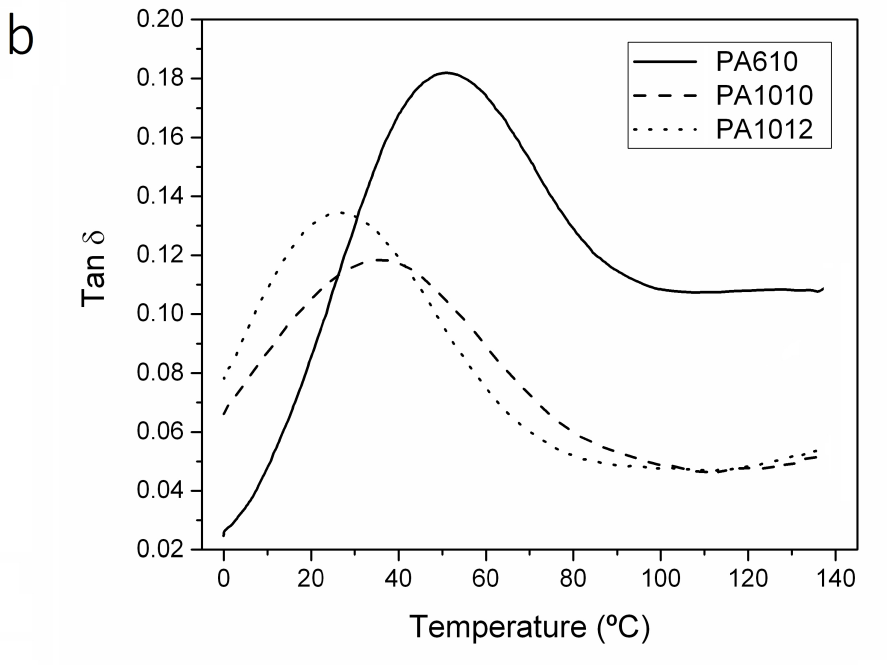
b
Tan δ
0.20
0.18
0.16
0.14
0.12
0.10
0.08
0.06
0.04
0.02
0
20
40
60
80
100
120
140
Temperature (ºC)
PA610
PA1010
PA1012

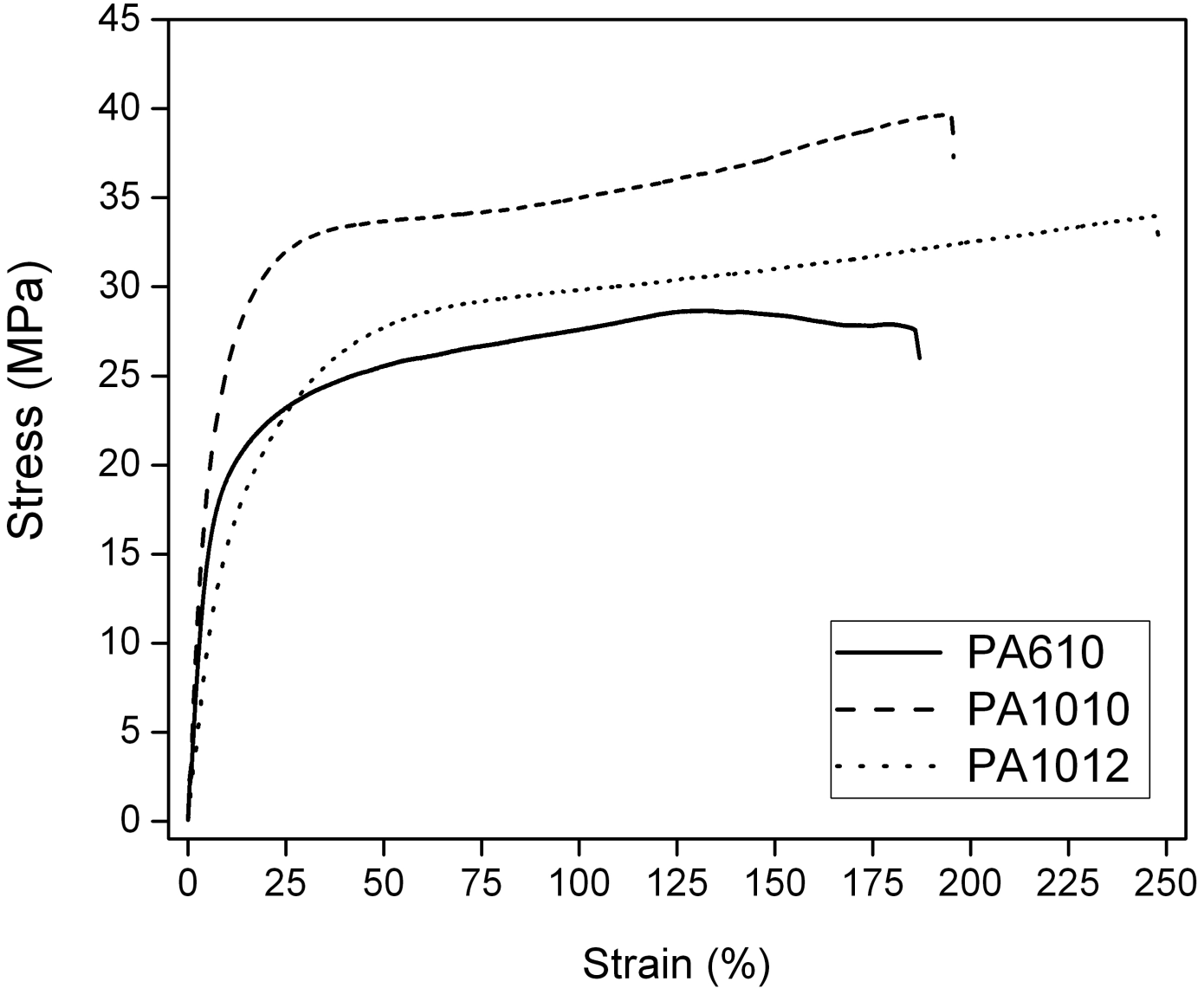
Stress (MPa)
Strain (%)
0
5
10
15
20
25
30
35
40
45
0
25
50
75
100
125
150
175
200
225
250
PA610
PA1010
PA1012

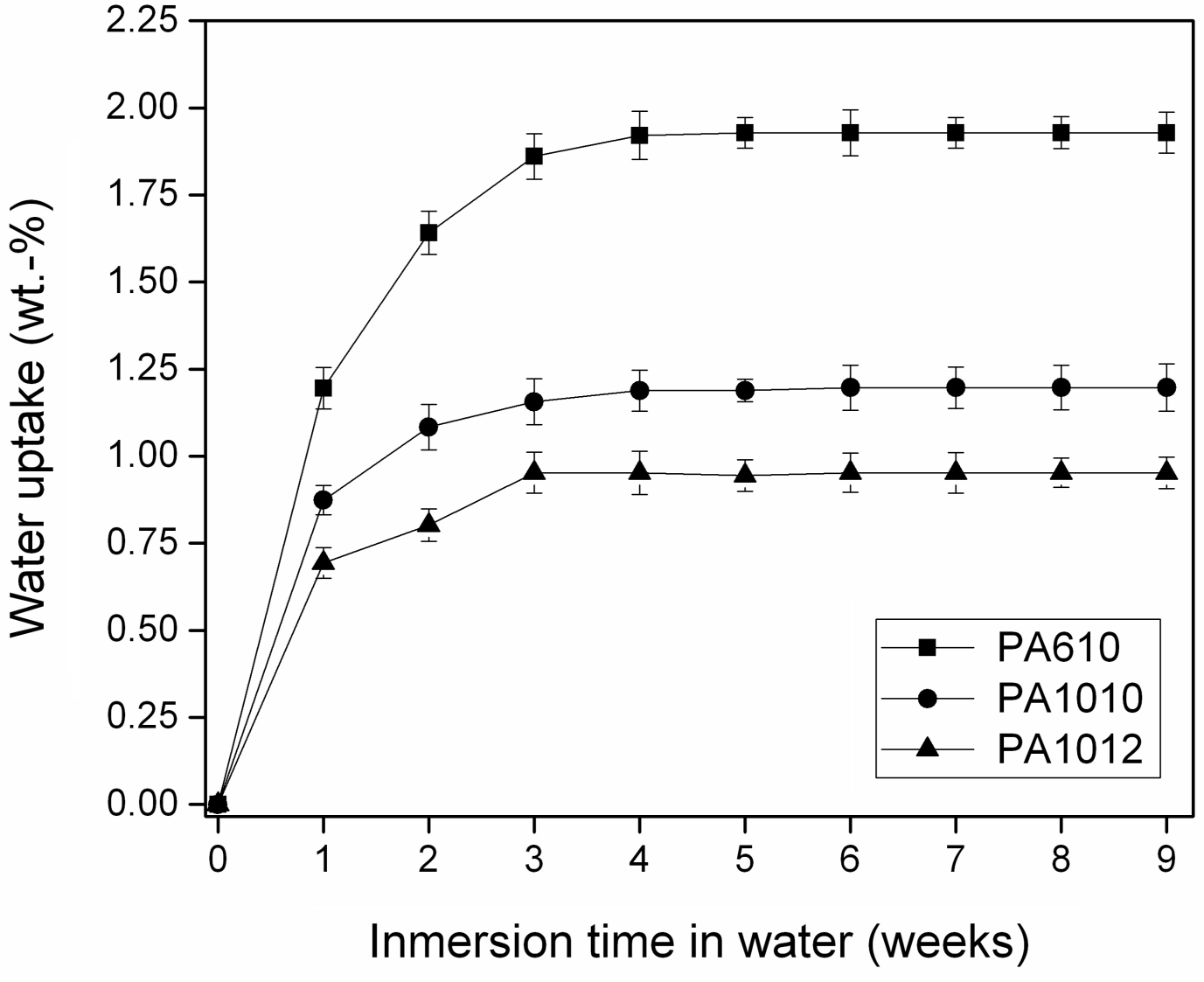
Water uptake (wt.-%)
2.25
2.00
1.75
1.50
1.25
1.00
0.75
0.50
0.25
0.00
0
1
2
3
4
5
6
7
8
9
Inmersion time in water (weeks)
PA610
PA1010
PA1012

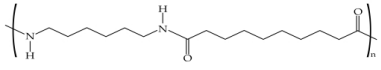

PA610

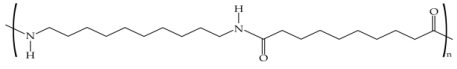

PA1010

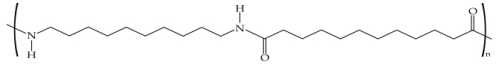

PA1012